https://doi.org/10.1016/j.atmosenv.2018.11.042

Meteorological Conditions for Severe Foggy Haze Episodes over North China in 2016-2017 Winter

Xin Li[1], Zhiqiu Gao[1-2]*, Yubin Li[1], Chloe Y. Gao[3], Jingzheng Ren[4], Xiaoye Zhang[5]

[1] Climate and Weather Disasters Collaborative Innovation Center, Key Laboratory for Aerosol-Cloud -Precipitation of China Meteorological Administration, School of Atmospheric Physics, Nanjing University of Information Science and Technology, Nanjing, 210044, China; lixin_91lx@126.com, liyubin@nuist.edu.cn

[2] State Key Laboratory of Atmospheric Boundary Layer Physics and Atmospheric Chemistry, Institute of Atmospheric Physics, Chinese Academy of Sciences, Beijing, 100029, China; zgao@mail.iap.ac.cn

[3] Department of Earth and Environmental Sciences, Columbia University, New York, NY 10027, USA; y.gao@columbia.edu

[4] Department of Industrial and Systems Engineering, The Hong Kong Polytechnic University, Hong Kong SAR, China; renjingzheng123321@163.com

[5] Chinese Academy of Meteorological Sciences, Beijing, 100081, China; xiaoye@camscma.cn

* Correspondence: Dr. Zhiqiu Gao, zgao@mail.iap.ac.cn; Tel.: +86-25-5869-5706

Abstract: This paper aims to identify the meteorological conditions of severe foggy haze events that frequently occurred over North China. We analyzed data collected at 162 ground observation stations operated by China Meteorological Administration (CMA), as well as data from National Centers Environmental Prediction (NCEP) over North China from December 1, 2016 to January 9, 2017. During this period, more than 72% of the regional mean atmospheric visibility was less than 10 km, with a minimum of 1.15 km. The analysis on atmospheric background fields revealed that during the pollution development-maintenance period there were southerlies and lower wind speed in the lower troposphere compared to that during the pollution dissipation period. Slow southerlies transported the southern pollutants to North China, while high pressure system at the 500 hPa level and increasing temperature (caused by air pollutant absorbed radiation) at 850 hPa suppressed the convection and led to pollutants accumulation over the ground. During the pollution dissipation period, there were northerlies and higher wind speed , and the fast northerlies quickly transported the pollutants. The analysis on the dynamic and thermodynamic effect suggests that the smaller horizontal wind vertical shear is attributed to 500 hPa decreased wind speed. The air pollutant warming effect on 850 hPa from absorbed solar radiation and cooling effect on near surface from reduced radiation near surface could lead to a larger correlation between atmospheric visibility and thermodynamic conditions for more than 76%. This coupling structure between air pollutant and thermodynamic situation provide favorable conditions for foggy haze events under air pollutant transport and weak vertical exchange conditions. Therefore, in order to predict foggy haze episodes in North China, we need to better understand its dynamics, especially for decreased middle level wind speed and lower level south flow.

Keywords: Foggy haze episodes; Meteorological conditions; North China; 2016-2017 winter

High light：slow southerlies near the surface; high pressure system at the 500 hPa; 500 hPa decreased wind speed caused weak horizontal wind vertical shear; air pollutant and thermodynamic conditions coupling structures.

1. Introduction

With increasing pollution sources from rapid urbanization and massive industrial production, foggy haze events, which cause low atmospheric visibility [1] and are mainly caused by particle matter (PM) [2], are becoming more frequent and severe in North China [3-4]. This serious environmental problem is even worse when coal is used for heating during the winter seasons [5-6]. So that, we should do more study on foggy haze process to reduce these increasing air pollution events.

Numerous studies investigated the pollution emission and transportation episodes together with the corresponding meteorological conditions in North China [7-12], and they found out the favorable meteorological conditions for haze events include low surface wind [4, 13], low planetary boundary layer

height [14-17], high relative humidity [18-20], strong temperature inversion [20-23], high pressure ridge, and much subsidence [23-24]. It was also implied that stable planetary boundary layer is conducive to the formation of haze [14, 16, 25]. In addition, the characteristics of the terrain in North China also play an important role. For instance, the location of Yan, Taihang mountains and the pollution sources in south areas led to more severe air pollution events when southerly winds prevail. [5, 8-11, 26-28]. Despite these known causal conditions, the dynamic and thermodynamic factors for foggy haze episodes in North China are not clear. To this end, we discuss the meteorological conditions here to determine the significant meteorological factors in foggy haze episode, which could be the theory basis of air pollution prediction and pollution control.

The objective of this paper is to quantify the impact of meteorological conditions on foggy haze episodes in North China by using daily ground observations and the NCEP final analysis (FNL) in North China from December 1, 2016 to January 9, 2017. The observational data and methods used are described in Section 2 of this study. Section 3 compares the mean synoptic situations during pollution development-maintenance and dissipation periods. Section 4 investigates the impact of meteorological factors, including dynamic and thermodynamic effect, on the daily evolution of foggy haze episodes. Section 5 discuss the evolution rule for meteorological conditions and air pollution process. Finally, the concluding remarks are given in Section 6.

2. Materials

2.1. Data

In this paper, we define area within 37-41°N and 114-119.5°E as North China (Figure 1). The following data were used: (1) Daily ground data collected at 162 China Meteorological Administration observational stations over North China from December 1, 2016 to January 9, 2017 and (2) NCEP FNL data in North China from December 1, 2016 to January 9, 2017, with a horizontal resolution of 1°×1° and a vertical resolution of 31 levels from 1000 hPa to 1 hPa. The ground observation data, including surface wind speed, wind direction, air temperature, relative humidity and atmospheric visibility, as well as FNL data were collected 4 times a day at 0200, 0800, 1400, and 2000 (Beijing time), respectively. Considering the significant correlation between air pollutants and atmospheric visibility[29], the variation of atmospheric visibility was used to reflect the evolution of foggy haze episodes in this study.

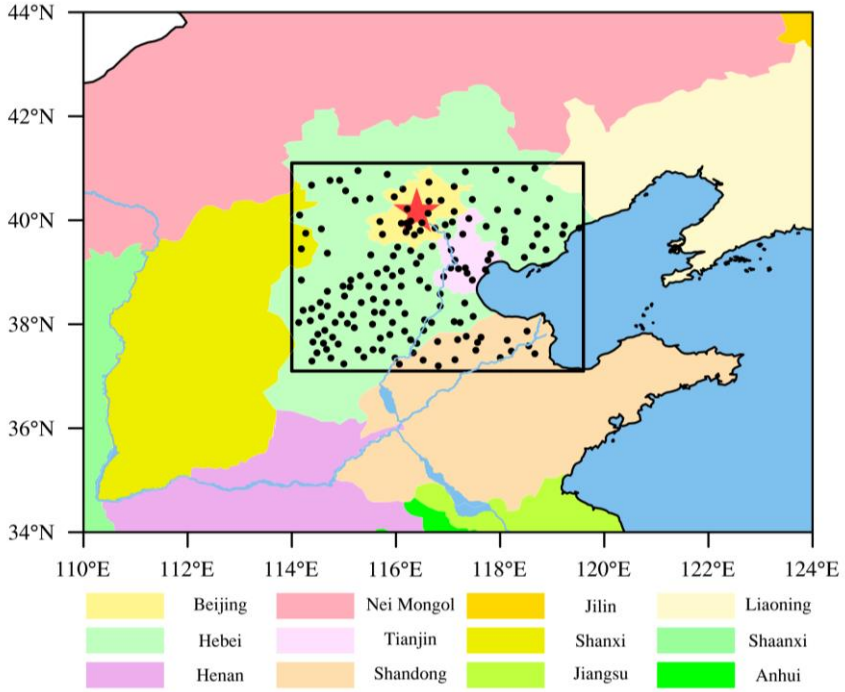

Figure 1. Map of North China, the locations of 162 observational stations are shown as black points. The black box represents the area of 37-41°N, 114-119.5°E.

2.2. Methods

In this study, we use the time average method to compare the mean synoptic patterns between air pollution development-maintenance and dissipation periods. In addition, the spatial mean method was also used to analyse the variation of weather conditions over North China during the observation period. Further, the correlation analysis and multivariate linear regression were applied to quantify the impact of weather conditions on the evolution of foggy haze episodes. In order to quantify the impact of dynamic and thermodynamic effects, a variety of indicators were discussed herein, including surface wind speed, vertical wind shear, dew-point deficit, vertical difference of pseudo-equivalent potential temperature, vertical difference of air temperature, K and A index. Both the K index and A index are applied to characterize the thermodynamic instability of atmosphere [30], and can be calculated through:

$$K = (T_{850} - T_{500}) + T_{d850} - (T - T_d)_{700} \quad (1)$$

$$A = (T_{850} - T_{500}) - \left[(T - T_d)_{850} + (T - T_d)_{700} + (T - T_d)_{500} \right] \quad (2)$$

where T and T_d are air temperature and dewpoint, respectively. The subscripts 850, 700, and 500 represent 850, 700, and 500 hPa, respectively.

3. Weather Background

The regional mean of surface wind speed, wind direction, air temperature, relative humidity and atmospheric visibility during the study period were presented in Figure 2. According to Figure 2a, we can find that the surface wind speed was relatively low with the maximum and mean wind speed of 3.56 ms^{-1} (at 1400 on December 5, 2016) and 0.76 ms^{-1}, respectively. Figure 2b reveals that the east (45°-135°), south (135°-225°), west (225°-315°) and north wind (0°-90° and 315°-360°) account for 14.06%, 27.40%, 18.12% and 40.31% of the regional mean surface wind directions during observation period, respectively. The regional mean air temperature (see Figure 2c) and relative humidity (see Figure 2d) both significantly varied with a diurnal circle, and the daily maximum (minimum) often occurred at about 1600 (0800) for air temperature while the opposite for relative humidity. The maximum, minimum and mean of regional mean air temperature (relative humidity) were 10.25 °C at 1500 on December 2, 2016 (94.59% at 0600 on December 20, 2016), -9.26 °C at 0800 on December 29, 2016 (24.26% at 1400 on December 1, 2016) and -0.56 °C (71.66%), respectively. Figure 2e shows the variation of atmospheric visibility, and more than 72.81% of visibility was lower than 10 km, which was implied to foggy haze episodes [29]. The visibility reached the minimum of 1.15 km (at 1500 on December 31, 2016) during air pollution period and increase to 24.80 km (at 1300 on December 9, 2016) for clean days. Combined with the variation of relative humidity presented in Figure 2d, we can concluded that the daily peak of relative humidity had an opposite variation compared to that of visibility. In other words, the daily maximum of relative humidity mainly corresponded to the daily minimum visibility.

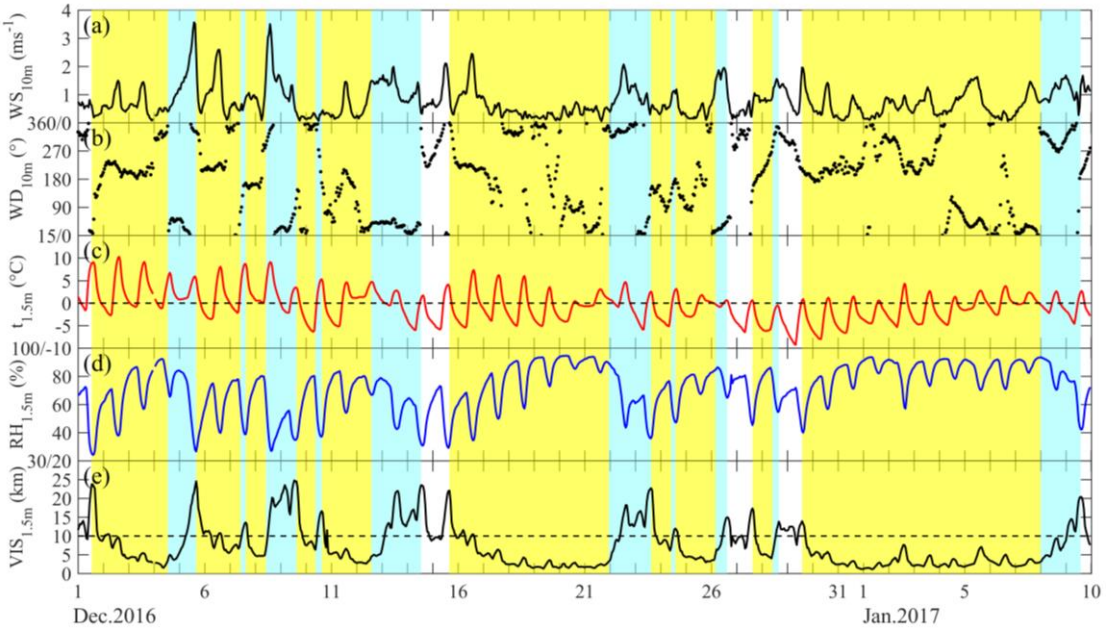

Figure 2. Temporal variations of regional mean (a) surface wind speed, (b) surface wind direction, (c) air temperature, (d) relative humidity, and (e) atmospheric visibility from December 1, 2016 to January 9, 2017 (Beijing time). The dashed line in (e) represents the 10 km visibility. The pollution development-maintenance and dissipation periods which are discussed in Section 3.1 are marked in yellow and blue, respectively.

Considering the significant correlation between atmospheric visibility and air pollution episodes, the air pollution development-maintenance period and dissipation period were categorized according to the decreasing and increasing trend of atmospheric visibility, respectively. The air pollution development-maintenance period started from the maximum visibility before a foggy haze process and ended when the visibility reached its minimum, and then it stabilized at around minimum with variation less than 2 km. In other words, the decreasing period (from maximum to minimum visibility) and the period that visibility increase from minimum to minimum+2km both belong to the air pollution development-maintenance period. The dissipation period started when the development-maintenance period ended, and continued until the visibility reached its maximum. To eliminate the effect of short-time pollution, pollution episodes with visibility smaller than 10 km and last for more than 12 hours were considered. During the observation period, there were 10 air pollution episodes, and the pollution development-maintenance and dissipation periods were marked in yellow and blue in Figure 2e, respectively. The corresponding mean wind speed, wind direction, air temperature, relative humidity and visibility for the 10 air pollution episodes were presented in Table 1. We found that the prevailed southern wind during the pollution development-maintenance period was lower in most pollution episodes, and during the air pollution dissipation period, there were always higher north wind. As for the 4th and 10th pollution episodes, the winds were too low, so the effects of wind directions were negligible. Owing to the weak radiation [31-33] during foggy haze episodes, the averaged near surface air temperature was smaller during pollution development-maintenance periods than during pollution dissipation periods. The relative humidity was usually larger during air pollution development-maintenance periods [3, 25]. In this study, there were 8 out of 10 pollution episodes (the 2ed-7th and 9th-10th episodes) that had larger mean relative humidity, and 6 of them showed a difference of mean relative humidity over 10% between pollution development-maintenance and dissipation periods. Therefore, during this observation period, the impact of relative humidity on foggy haze episodes was significant near the surface. The mean atmospheric visibility is often smaller under pollution development-maintenance stage than under dissipation stage, but there are 2 pollution episodes that have larger averged atmopheric visibility (>10 km) during air pollution development-maintenane periods. This could be caused by the short time intervals and the large maximum visibility at the beginning of the 2 pollution development-maintenane periods.

Table 1. The occurrence date, mean wind speed (WS_{avg}), wind direction (WD), air temperature (t_{avg}), relative humidity (RH_{avg}) and atmospheric visibility (VIS_{avg}) for 10 air pollution episodes. The variables during air pollution dissipation period were showed in bracket.

Air pollution development-maintenance periods (dissipation periods)					
Date (Beijing time)	Ws_{avg} (ms^{-1})	WD (°)	t_{avg} (°C)	RH_{avg} (%)	VIS_{avg} (km)
1 Dec. 13:00 – 4 Dec. 13:00 (4 Dec. 13:00 – 5 Dec. 16:00)	0.43 (1.38)	214.65 (8.93)	2.68 (3.02)	67.64 (68.31)	6.77 (9.89)
5 Dec. 16:00 – 7 Dec. 10:00 (7 Dec. 10:00 – 7 Dec. 15:00)	0.60 (0.51)	239.14 (136.98)	0.62 (6.93)	60.58 (46.21)	9.78 (11.56)
7 Dec. 15:00 – 8 Dec. 10:00 (8 Dec. 10:00 – 9 Dec. 15:00)	0.54 (1.23)	175.54 (358.20)	2.14 (2.42)	69.06 (43.95)	6.39 (18.54)

9 Dec. 15:00 – 10 Dec. 09:00 (10 Dec. 09:00 – 10 Dec. 15:00)	0.13 (0.07)	13.11 (248.22)	-2.96 (2.47)	65.31 (47.91)	10.83 (12.60)
10 Dec. 15:00 – 12 Dec. 14:00 (12 Dec. 14:00 – 14 Dec. 13:00)	0.14 (1.18)	111.30 (34.58)	0.41 (-0.35)	71.04 (61.95)	5.26 (13.22)
15 Dec. 16:00 – 21 Dec. 23:00 (21 Dec. 23:00 – 23 Dec. 15:00)	0.13 (0.92)	223.77 (346.93)	-0.68 (-0.40)	77.92 (63.30)	4.18 (13.33)
23 Dec. 15:00 – 24 Dec. 10:00 (24 Dec. 10:00 – 24 Dec. 14:00)	0.47 (0.99)	124.00 (161.75)	-2.80 (1.15)	64.19 (53.88)	10.35 (10.00)
24 Dec. 14:00 – 26 Dec. 04:00 (26 Dec. 04:00 – 26 Dec. 15:00)	0.12 (1.68)	120.54 (27.35)	-0.44 (-0.22)	74.22 (78.80)	4.91 (9.56)
27 Dec. 15:00 – 28 Dec. 10:00 (28 Dec. 10:00 – 28 Dec. 16:00)	0.68 (1.23)	207.98 (327.83)	-4.48 (-1.57)	74.36 (63.90)	7.11 (9.74)
29 Dec. 14:00 – 8 Jan. 0000 (8 Jan. 00:00 – 9 Jan. 14:00)	0.05 (0.91)	303.24 (307.25)	-1.65 (-0.87)	82.97 (78.28)	3.34 (9.30)
Average of all pollution development-maintenance periods	0.22	193.83	-0.72	70.73	6.89
(Average of all pollution dissipation periods)	(0.62)	(5.71)	(1.26)	(60.65)	(11.77)

3.1. Synoptic Situation

Depending on the visibility variation (see Figure 2e), the averaged synoptic weather situations under pollution development-maintenance and dissipation periods were calculated (as presented Figures 3-5) to explore the influence of the synoptic situation. The mean geopotential heights, air temperature and winds in middle troposphere (500 hPa) were shown in Figures 3a (development-maintenance period) and 3b (dissipation period). It can be seen that westerlies and northwesterlies prevailed in middle troposphere during air pollution development-maintenance and dissipation periods, respectively. The synoptic difference between these two periods, as presented in Figure 3c, showed that the difference of geopotential height, wind speed and air temperature in North China have positive, negative and positive effects, respectively. The positive geopotential height difference indicated a higher pressure in North China during development-maintenance period. Usually, the higher pressure and weak convection were often conducive to the formation of air pollution [23-24]. In this study, the middle troposphere higher pressure could weaken cold advection, which may be not the key factor for increasing temperature discussed later in section 3.2 and was caused by north wind, to increase the temperature in middle troposphere (1-4 °C air temperature increment showed in Figure 3c). Then the reduced temperature gradient can suppress convection and eventually contribute to the pollutants accumulation under near surface[34].

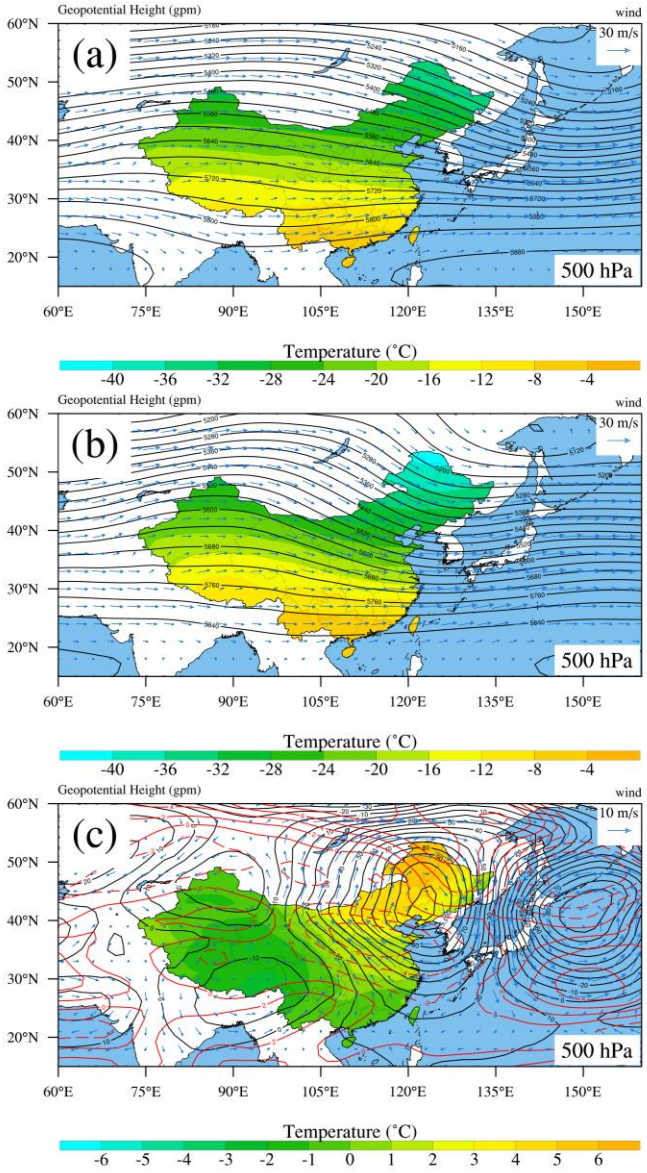

Figure 3. Averaged geopotential heights (black lines; units: gpm), air temperature (shadings; units: °C) and winds (blue vectors) at 500 hPa during (a) air pollution development-maintenance and (b) dissipation periods. The geopotential height (black lines; units: gpm), wind speed (red lines; units: ms^{-1}) and air temperature (shadings; units: °C) difference between two periods at 500 hPa were showed in Figure 3c. Real and dotted red lines are for positive and negative anomalies, respectively.

Figures 4a and Figure 4b showed the mean geopotential heights, air temperature and winds in lower troposphere (925 hPa) under pollution development-maintenance and dissipation periods, respectively. As presented in Figure 4, there was a high-pressure system to the southeast of North China and the southerlies prevailed when pollution aggravated. During the pollution dissipation period, a high-pressure system was at the northwest of North China, and the higher north wind prevailed in North China. The synoptic difference between these two periods (Figure 4c) showed the negative and positive wind speed and air temperature difference in North China, respectively. In other words, there were northerlies and higher wind speed when air pollution dissipated and southerlies and lower wind speed when pollution aggravated and maintained in North China. Considering the amount of industries and pollution sources to the south of North China [10, 27], the lower south wind could transport the pollutants from south to North China and then accumulate here. This phenomenon in North China has been confirmed by previous studies [11, 28]. Additionally, the positive air temperature difference (1-3 °C) indicated a warm advection in lower troposphere during air pollution development-maintenance period.

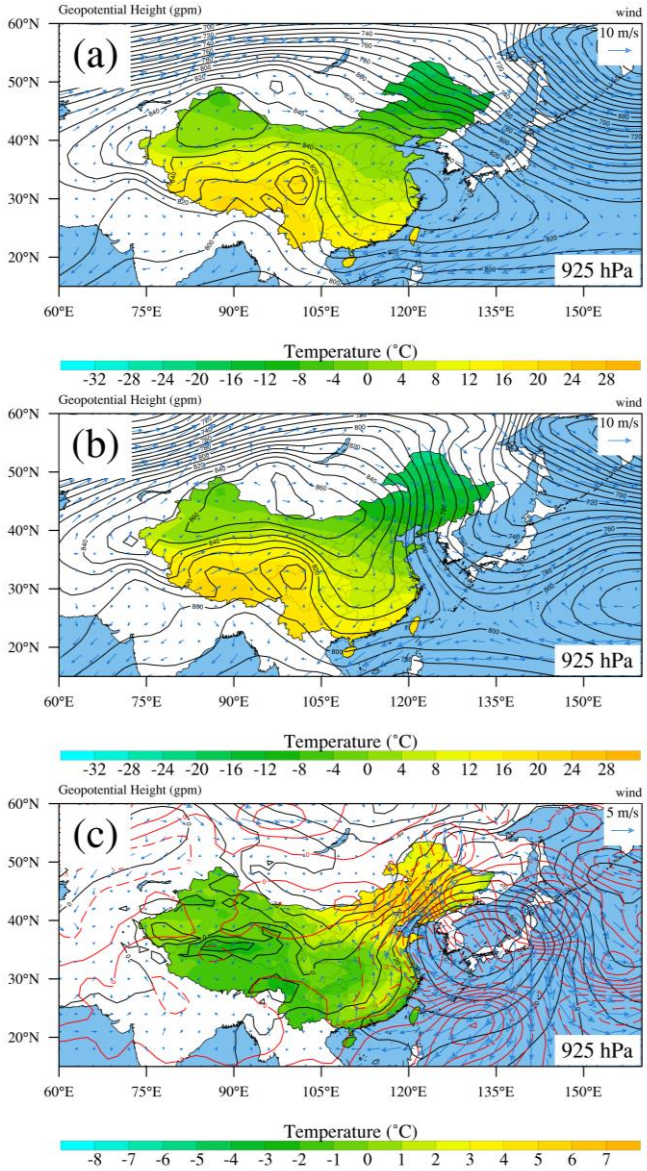

Figure 4. Averaged geopotential heights (black lines; units: gpm), air temperature (shadings; units: °C) and winds (blue vectors) at 925 hPa during (a) air pollution development and (b) dissipation periods. The geopotential height (black lines; units: gpm), wind speed (red lines; units: ms^{-1}) and air temperature (shadings; units: °C) difference between two periods at 925 hPa were showed in Figure 4c. Real and dotted red lines are for positive and negative anomalies, respectively.

Figures 5a and Figure 5b showed the mean 925 hPa relative humidity and 10m winds under pollution development-maintenance and dissipation periods, respectively. Similar to the winds at 925 hPa, southerlies and lower wind (higher northerlies) prevailed when air pollution aggravated and maintained (dissipated). These situations were confirmed by Figure 5c which showed the difference between air pollution development-maintenance and dissipation periods. The mean relative humidity difference was about -10% to -20% in North China, and it indicated a lower relative humidity in 925 hPa in North China during air pollution development-maintenance period. As the saturated vapor pressure increases with increasing air temperature, this smaller relative humidity may be caused by the strong warm advection in lower troposphere (see Figure 4c) when pollution developed[35]. From the above analysis, the joint influence of higher pressure in middle troposphere and southern wind in lower troposphere led to the foggy haze episodes.

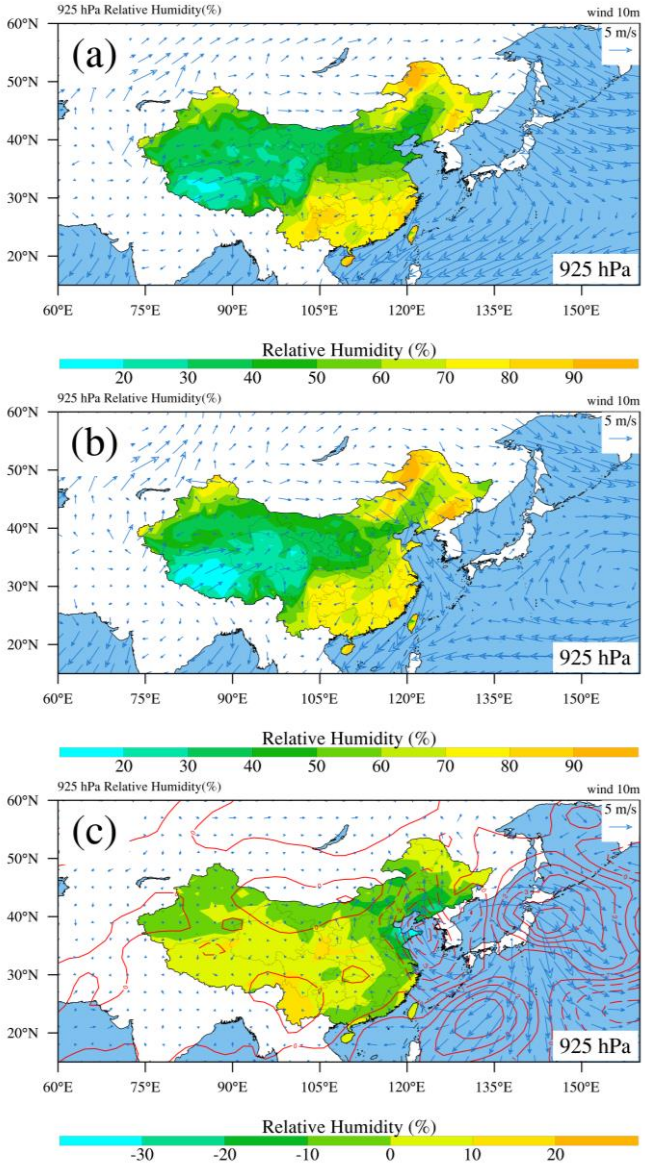

Figure 5. The mean 925 hPa relative humidity (shadings; units: %) and 10m winds (blue vectors) under (a) pollution development and (b) dissipation period. The mean 925 hPa relative humidity (shadings; units: %) and 10m winds (blue vectors) difference between two periods was showed in Figure 5c. Real and dotted red lines are for positive and negative anomalies, respectively.

3.2. Vertical Profiles

In order to reveal the vertical structures of atmospheric background fields, the vertical distribution of regional mean horizontal wind speed (see Figure 6a), air temperature (see Figure 6b) relative humidity (see Figure 6c) and the difference of these three variables (see Figure 6d, 6e and 6f) between air pollution development-maintenance and dissipation periods were investigated. According to Figure 6a, under both air pollution development-maintenance and dissipation stages, the zonal wind was westerly and increased with height. The zonal wind speed difference between pollution development-maintenance and dissipation stages was positive below 750 hPa while negative from 700 hPa to 150 hPa. During air pollution development period, the southern meridional wind gradually decreased with the height increasing and turned to north at 800 hPa. While under air pollution dissipation stage, the northern meridional wind increased from 3.52 ms^{-1} at 1000 hPa to 7.20 ms^{-1} at 800 hPa and then almost stayed at 7.50 ms^{-1} from 800 to 300 hPa. The air temperature was higher below 300 hPa during pollution development-maintenance period. The relative humidity profiles

showed an opposite variation for two stages below 900 hPa, that is the relative humidity decreased with height during development-maintenance period while increased with height for dissipation stage.

Figure 6d showed the negative wind speed difference between two stages, and the maximum and minimum difference was -6.37 ms^{-1} at 400 hPa and -0.28 ms^{-1} at 150 hPa, respectively. From 1000 hPa to 900 hPa (lower troposphere) and from 400 hPa to 150 hPa (higher troposphere), the wind speed difference decreased with height, while from 900 hPa to 400 hPa, the difference increased with height. Combining the results presented in Figure 4a, the height-decreasing difference between two stages below 900 hPa was mainly caused by the height-increasing western zonal wind during air pollution development-maintenance period. During this period, the lower south wind speed in troposphere especially in the lower troposphere transported the southern pollutants north and was conducive to its accumulation here[10]. The higher wind speed was conducive to the dissipation of pollution.

The vertical distribution of regional mean air temperature (see Figure 6e) difference between air pollution development-maintenance and dissipation periods showed the positive values below 300 hPa with a maximum of 5.46 °C at 800 hPa. Combined with the wind profile presented in Figure 6a, the height-decreasing south wind speed should introduce a height-decreasing warm advection. However, there is a height-increasing temperature difference below 800 hPa. Considering the air pollutant solar radiation absorbing effect, the near surface weak radiation condition as well as upper atmosphere larger radiation both help form this temperature inversion during the pollution development-maintenance period. The peak difference corresponded to the meridional wind shift and less pollutant upon atmosphere boundary layer. The height-increasing temperature difference below 800 hPa implied a more stable lower troposphere, and suppressed the convection during pollution development-maintenance period. This weakened convection was conducive to the accumulation of pollutants near the surface[34].

The vertical distribution of regional mean relative humidity (Figure 6f) difference between air pollution development-maintenance and dissipation periods shows the negative values below 400 hPa with the maximum of 16.67% at 850 hPa. The south wind usually transported the humid and warm air mass and increased the relative humidity. In this study, the increased relative humidity difference between two stages was conducted by weakened water vapor support caused by weakened south meridional wind, as well as increased saturated vapor pressure caused by increased air temperature. The negative relative humidity difference in troposphere between two stages indicated the slight influence of water vapor conditions on the foggy haze episodes during observation period. Therefore, although as pointed out in previous studies that high relative humidity is more inclined to form haze [8, 20], this study found that the wind and temperature conditions are sometimes more decisive for the haze formation in North China.

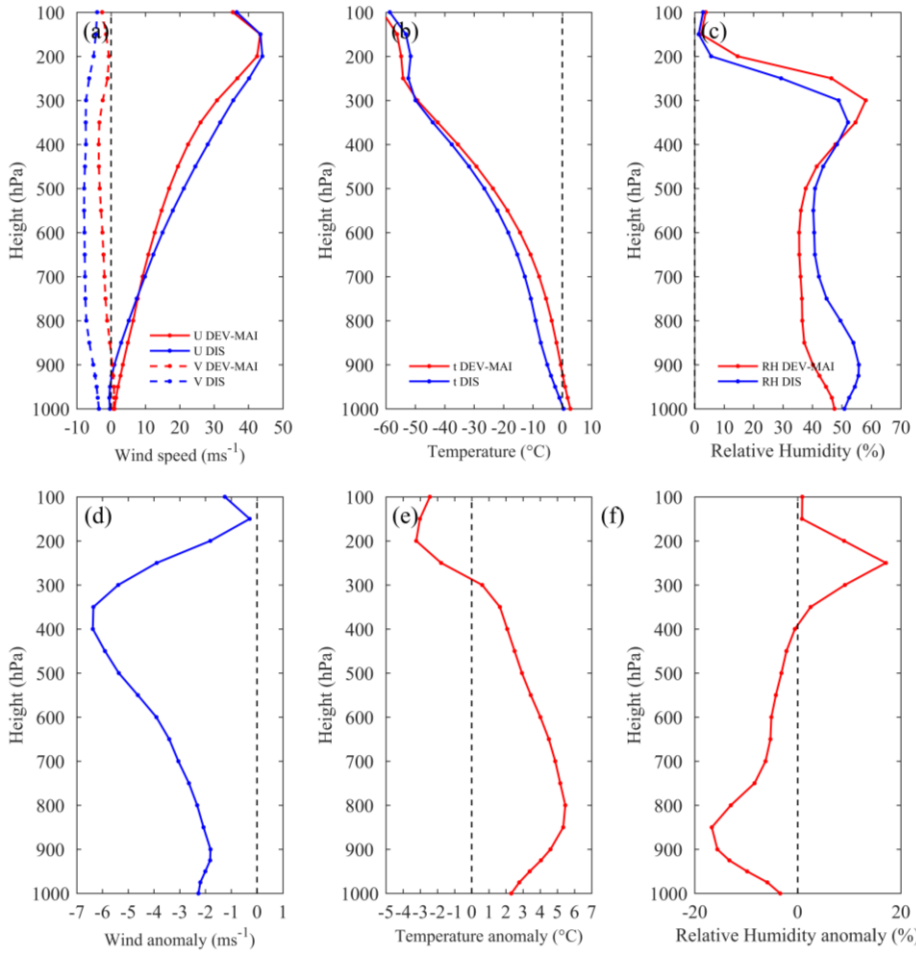

Figure 6. Vertical distributions of (a) horizontal wind (the U and V represent the zonal wind and meridional wind, respectively), (b) air temperature, and (c) relative humidity during air pollution development-maintenance and dissipation periods. The wind speed, air temperature, and relative humidity difference between two stages was showed in (d), (e), and (f), respectively.

4 Impact of Meteorological Factors

In order to investigate the the impacts of weather condition on the evolution of foggy haze episodes, we studied the meteorological conditions, including dynamic effect and thermodynamic effect, from December 1, 2016 to January 9, 2017 in this section.

4.1. Dynamic Effect

The surface wind and vertical shear of horizontal wind represent the outward horizontal transport and the vertical diffusion capacity, respectively. To identify the dynamic effect on the evolution of foggy haze episodes, this section presented the daily evolution of surface wind speed (Figure 7a) and the vertical shear of horizontal wind between 850 hPa and 500 hPa (Figure 7b) as well as the atmospheric visibility in Figure 7. The surface wind speed shows a small correlation coefficient of 0.31 with the atmospheric visibility, which is below the 0.05 confidence level. Meanwhile the vertical shear of horizontal wind between 850 hPa and 500 hPa shows a correlation coefficient of 0.33 with atmospheric visibility, and it slightly exceeds 0.05 confidence level. The higher wind speed or stronger vertical shear transport the pollutants outward, reduce the ground pollutants concentration and increase atmospheric visibility; while lower wind speed or weaker vertical shear with weaker transportation capacity make the pollutants accumulate near surface and decrease the atmospheric visibility[6].

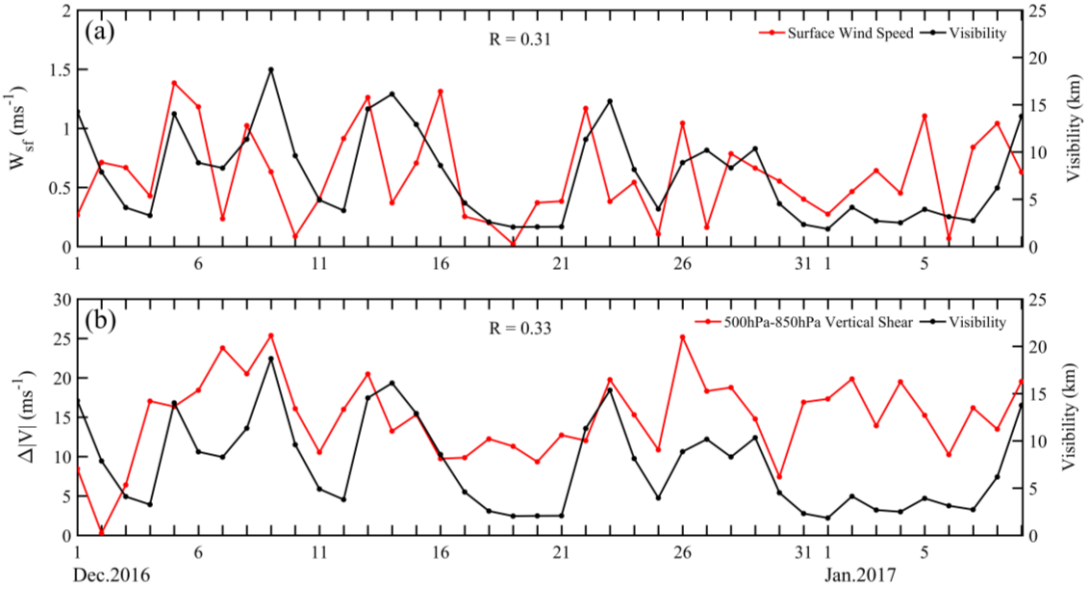

Figure 7. Daily evolutions of the surface wind speed (a) and vertical shear of horizontal winds (b) between 500 and 850 hPa as well as atmospheric visibility (black lines) averaged in North China from December 1, 2016 to January 9, 2017 (Beijing time).

4.2. Thermodynamic Effect

Both K and A indexes are the major indicators frequently used in weather forecast operations to determine the stability of atmospheric stratification [30]. To identify the thermodynamic impacts, the daily evolution of K index (Figure 8a) and A index (Figure 8b) as well as atmospheric visibility were investigated. It is apparent that the K index shows a negative correlation coefficient of -0.33 (slightly exceeding 0.05 confidence level) with atmospheric visibility. while the A index shows a poor correlation with atmospheric visibility (correlation coefficient of -0.06). Due to the stability of middle and lower troposphere stratification that reflected by K index, the negative correlation between K index and atmospheric visibility indicates the more unstable the middle and lower troposphere, the smaller the near surface visibility. Considering that the A index indicates not only the stability but also the water vapor saturation conditions in the middle and lower troposphere (as shown in equation 2), the poor correlation between A index and atmospheric visibility should be caused by the insigfinicant influence of water vapor conditions in this foggy haze episodes.

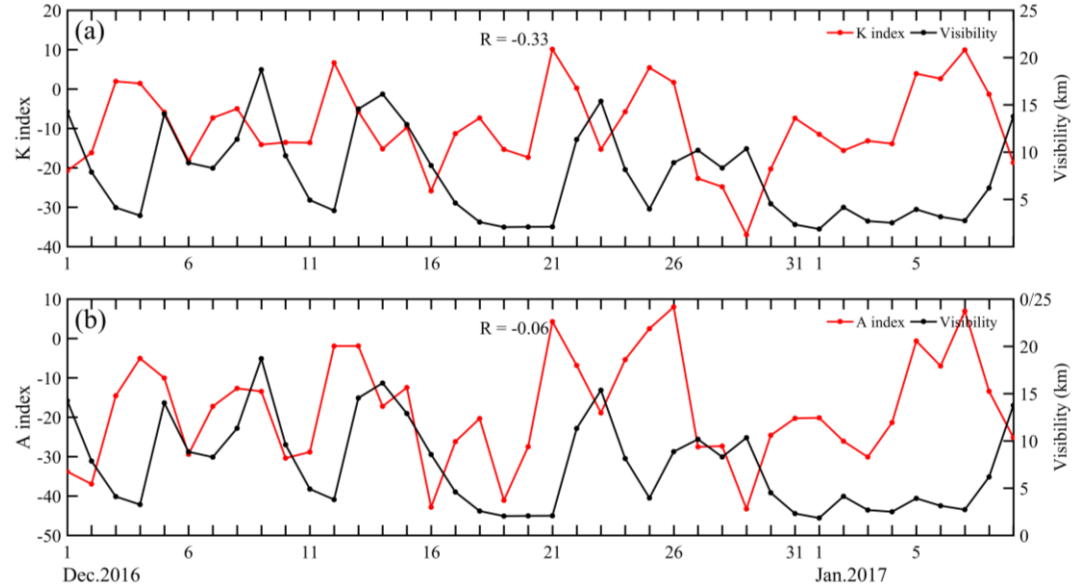

Figure 8. Daily evolutions of K index (a) and A index (b) as well as atmospheric visibility (black lines) averaged in North China from December 1, 2016 to 9 January 9, 2017 (Beijing time).

Figure 9 showed the daily evolution of vertical difference of the pseudo-equivalent potential temperature between 850 and 1000 hPa (Figure 9a), dewpoint deficit at 925 hPa (Figure 9b) and the vertical difference of air temperature between 925 and 1000 hPa (Figure 9c) as well as atmospheric visibility. The pseudo-equivalent potential temperature gradient and air temperature gradient show negative correlation (both exceed 0.01 confidence level) with atmospheric visibility, with correlation coefficients of -0.73 and -0.73, respectively. Whereas the dewpoint deficit shows poor correlation with atmospheric visibility. Due to the lower troposphere stability reflected by pseudo-equivalent potential temperature gradient (between 850 and 1000 hPa) and air temperature gradient (between 925 and 1000 hPa), the negative correlation implies the more stable the lower troposphere, the smaller the atmospheric visibility. It reflects the thermodynamic convection influences the near surface pollutants accumulation. Considering the water vapor conditions indicated by dewpoint deficit at 925 hPa, the water vapor conditions played an "less important" role in these pollution episodes.

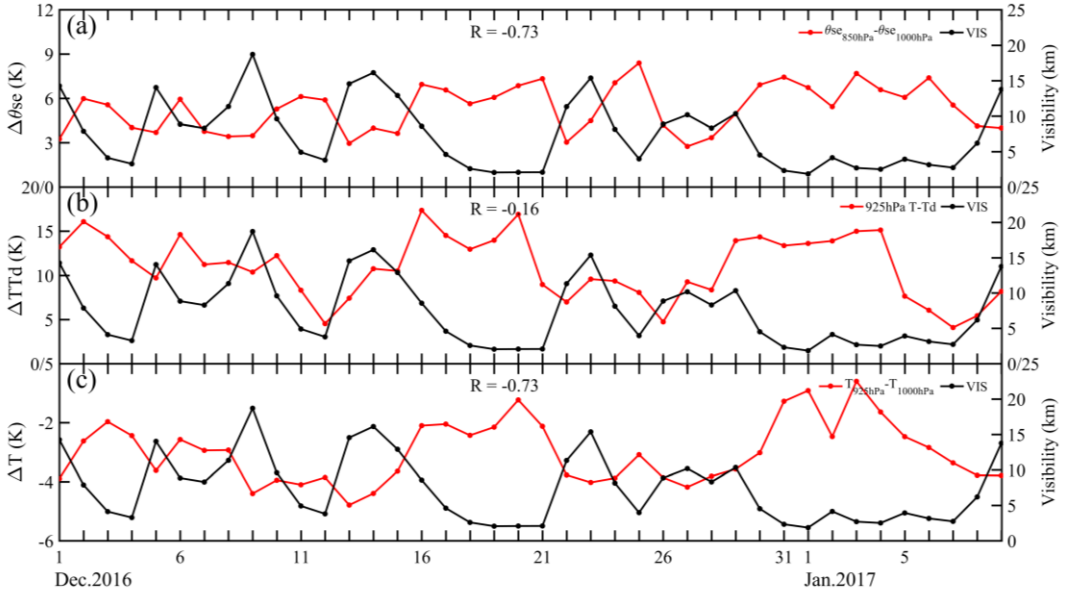

Figure 9. Daily evolutions of vertical difference of pseudo-equivalent potential temperature (a) between 850 and 1000 hPa, dewpoint deficit at 925 hPa (b) and the vertical difference of air temperature between 925 and 1000 hPa (c) as well as atmospheric visibility (black lines) averaged in North China from December 1, 2016 to January 9, 2017 (Beijing time).

4.3. Regression Analysis of Meteorological Factors

In order to further quantify the influence of the meteorological conditions on the evolution of the air pollution episodes, we used the multiple linear regression method to quantify the impact of meteorological dynamic and thermodynamic effect in Figure 10. The daily variation of visibility calculated by regression equation based on dynamic and thermodynamic factors matches very well with the observed visibility as the determination coefficient is 0.79. additionally, there is a poor (good) consistency between dynamic-regressed (thermodynamic-regressed) and observed visibility with the determination coefficient of 0.18 (0.76). These regressed results indicate that the daily variation of the visibility regressed from meteorological factors can effectively explain approximately 79% daily variation of observed visibility. While approximately 76% atmospheric visibility variation can be attributed to the thermodynamic effect, and dynamic effect has a small contribution to the evolution of pollution episodes.

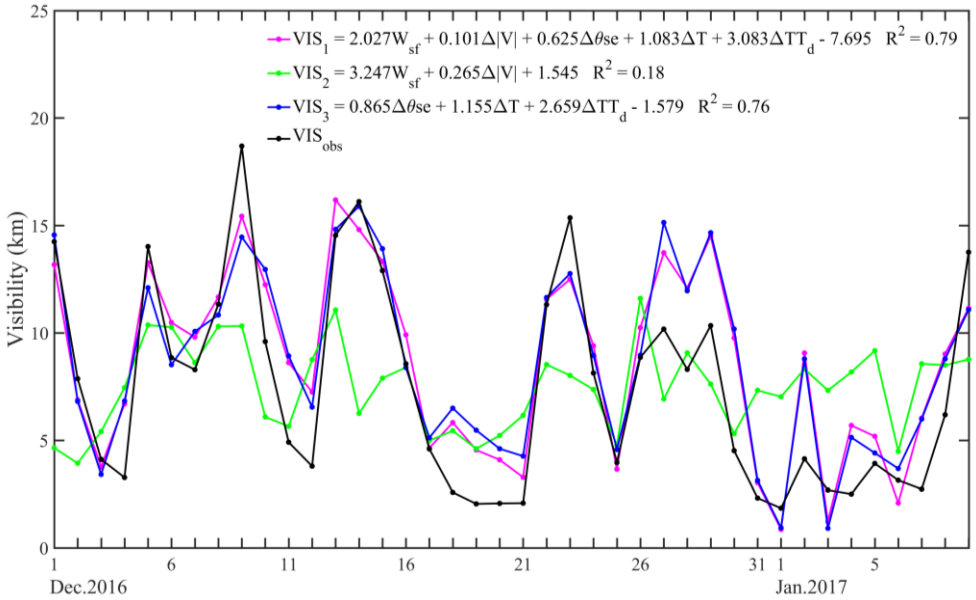

Figure 10. Daily variation of linearly regressed visibility by multivariate of the dynamic and thermodynamic meteorological factors and observed visibility averaged in North China from December 1, 2016 to January 9, 2017 (Beijing time).

5. Meteorological Factors Evolution

The above analysis on dynamic and thermodynamic conditions reflects the significant or slight synchronization between meteorological factors and atmospheric visibility during foggy haze episodes in North China. However, it is unclear how the meteorological factors affect the air pollution process and what the key processes for the occurrence of foggy haze episodes are. To this end, here we focus on one air pollution episode during December 15 to 23, 2017 with less atmospheric visibility variation during air pollution period.

5.1. Meteorological Conditions Analysis

Figure 11 displayed the 500-850 hPa horizontal wind vertical shear (Figure 11 a-c), 850-1000 hPa pseudo-equivalent potential temperature gradient (Figure 11 d-e) and relative humidity at 925 hPa (Figure 11 f-h) with surface wind and atmospheric visibility on the development (1400 on December 15), maintenance (1400 on December 19) and dissipation (1400 on December 22) stage of foggy haze episode, respectively. The data at noon were selected based on the well-developed boundary layer. In contrast to the values (16-22 ms^{-1} and 0-2 K) at 1400 on December 15, the markedly reduced wind shear (10-16 ms^{-1}) and increased pseudo-equivalent temperature gradient (2-6 K) at 1400 on December 19, unfolded the significantly different meteorological conditions between air pollution day and clean days. This is consistent with the positive (negative) correlation between wind shear (pseudo-equivalent potential temperature gradient) and atmospheric visibility showed in Figure 7 and Figure 9. However, the relative humidity did not display a significant evolution tendency for the near stable values of 30-60% on December 15 and 19. This phenomenon again proves the slight influence of humidity on this foggy haze episode.

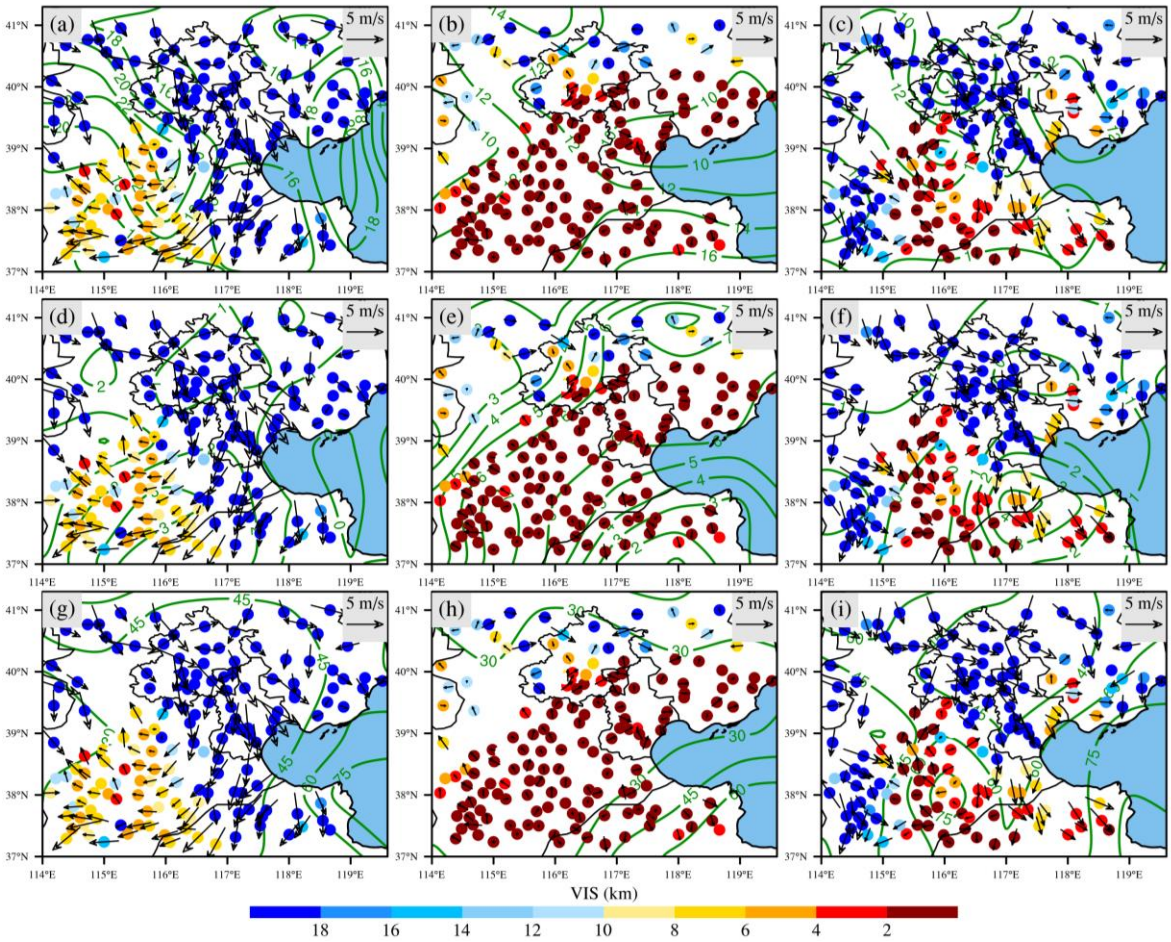

Figure 11. The 500-850 hPa horizontal wind vertical shear (a-c, ms^{-1}), 850-1000 hPa pseudo-equivalent potential temperature difference (d-e, K) and relative humidity at 925 hPa (f-h, %) with surface wind and atmospheric visibility on the development (1400 December 15, left panels), maintenance (1400 December 19, centre panels) and dissipation (1400 December 22, right panels) stage of foggy haze episode in North China from December 15 to 23, 2016 (Beijing time).

We explored the main cause for the markedly reduced wind shear on foggy haze maintenance period in Figure 12, it present the 500 hPa (Figure 12 a-c) and 850 hPa (Figure 12 d-f) wind speed at 1400 on December 15, 19 and 22. We found that two level wind speed both reduced from 24-26 ms^{-1} at 500 hPa and 6-10 ms^{-1} at 850 hPa (1400 December 15) to 12-20 ms^{-1} and 2-6 ms^{-1} (1400 December 19), respectively. However, the wind speed at 500 hPa decreased more significantly compared to that in the lower level. This wind reduction indicated that the decreased horizontal wind vertical shear was mainly caused by the decreased middle level wind speed, which is also shown in Figure 3. This reduced wind shear as well as the reduced lower wind speed both favor the accumulation of near surface air pollutant and contribute to the occurrence of air pollution events.

Similarity, Figure 13 showed the pseudo-equivalent potential temperature at 850 hPa (Figure 13 a-c) and 1000 hPa (Figure 13 d-f) with atmospheric visibility at 1400 on December 15, 19 and 22. Also, both the two level pseudo-equivalent potential temperature increased with the values from around 274-282 K (850 hPa) and 274-282 K (1000 hPa) on December 15 to the values of 290-292 K (850 hPa) and 282-292 K (1000 hPa) on December 19. Additionally, the values at 850 hPa increased more significantly than those at 1000 hPa. To further investigate the cause of the evaluation of pseudo-equivalent potential temperature, Figure 14-15 showed the air temperature (Figure 14) and specific humidity (Figure 15), which are factors of the pseudo-equivalent potential temperature, at 850 hPa (a-c) and 1000 hPa (d-f) with atmospheric visibility at 1400 on December 15, 19 and 22. Similar to pseudo-equivalent potential temperature, the air temperature also showed significant decreasing trend from 260-268 K (850 hPa) and 270-278 K (1000 hPa) at 1400 on December 15 to 272-276 K (850 hPa) and 278-282 K (1000 hPa) at 1400 on December 19. While the specific humidity also increased from 0.8-1.6 g kg^{-1} (850 hPa) and 1.0-2.0 g kg^{-1} (1000 hPa) on December 15 to

1.2-1.8 g kg^{-1} (850 hPa) and 1.6-3.8 g kg^{-1} (1000 hPa) on December 19. The larger intensification of pseudo-equivalent potential temperature at 850 hPa is attributed to greater air temperature increase and less specific humidity increase. While the smaller increasing of pseudo-equivalent potential temperature at 1000 hPa is attributed to the small air temperature increase and greater specific humidity increase. Therefore, the greater intensification of pseudo-equivalent potential temperature at 850 hPa is mainly controlled by the air temperature increase. In other words, the increased pseudo-equivalent potential temperature gradient at air pollution period could be attributed to the air temperature change. Meanwhile, the air temperature situation is mostly changed by the air pollutant absorb radiation effect discussed in section 3 (Figure 3-6), so that the increased pseudo-equivalent potential temperature gradient is introduced by air pollutant accumulation. The increasing concentration corresponds to a more stable structure with greater pseudo-equivalent potential temperature gradient.

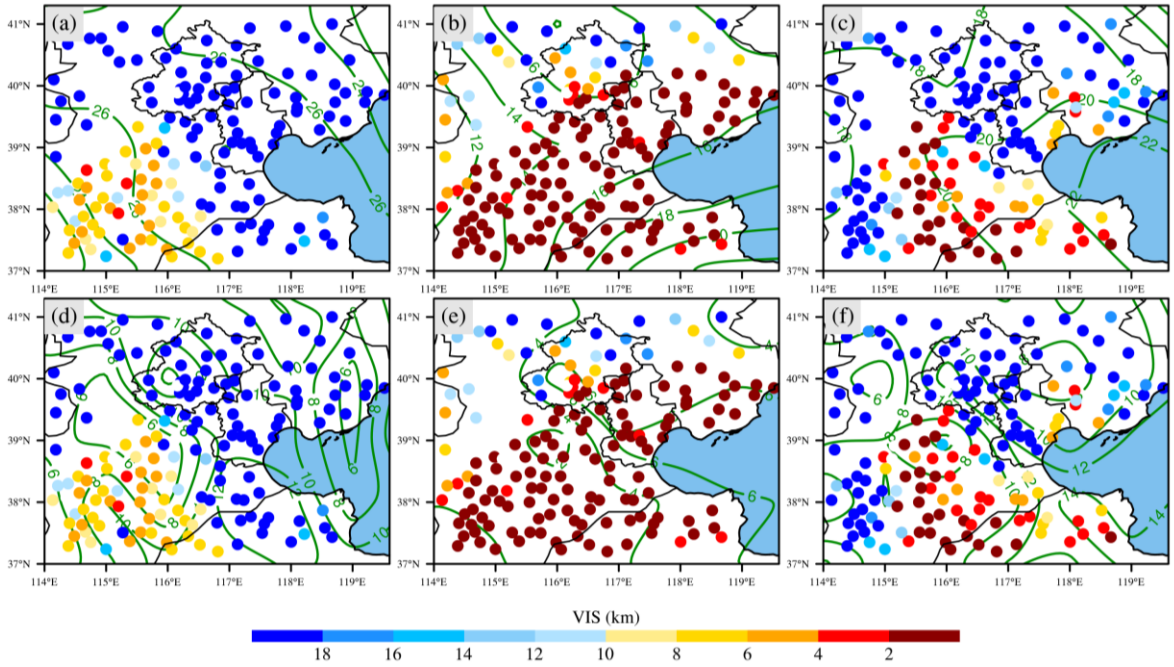

Figure 12. The 500 hPa (a-c) and 850 hPa (d-f) wind speed (ms^{-1}) as well as atmospheric visibility at 1400 on December 15 (left panels), 19 (centre panels) and 22 (right panels), 2016 in North China.

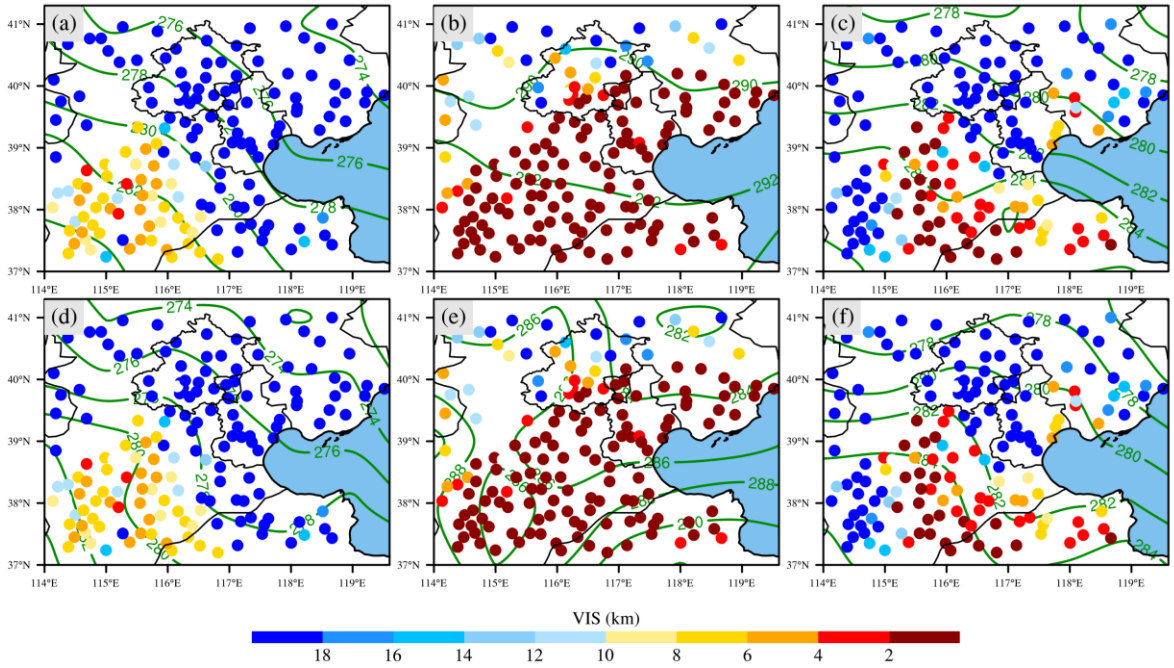

Figure 13. The pseudo-equivalent potential temperature (K) at 850 hPa (a-c) and 1000 hPa (d-f) with visibility at 1400 on December 15 (left panels), 19 (centre panels) and 22 (right panels), 2016 in North China.

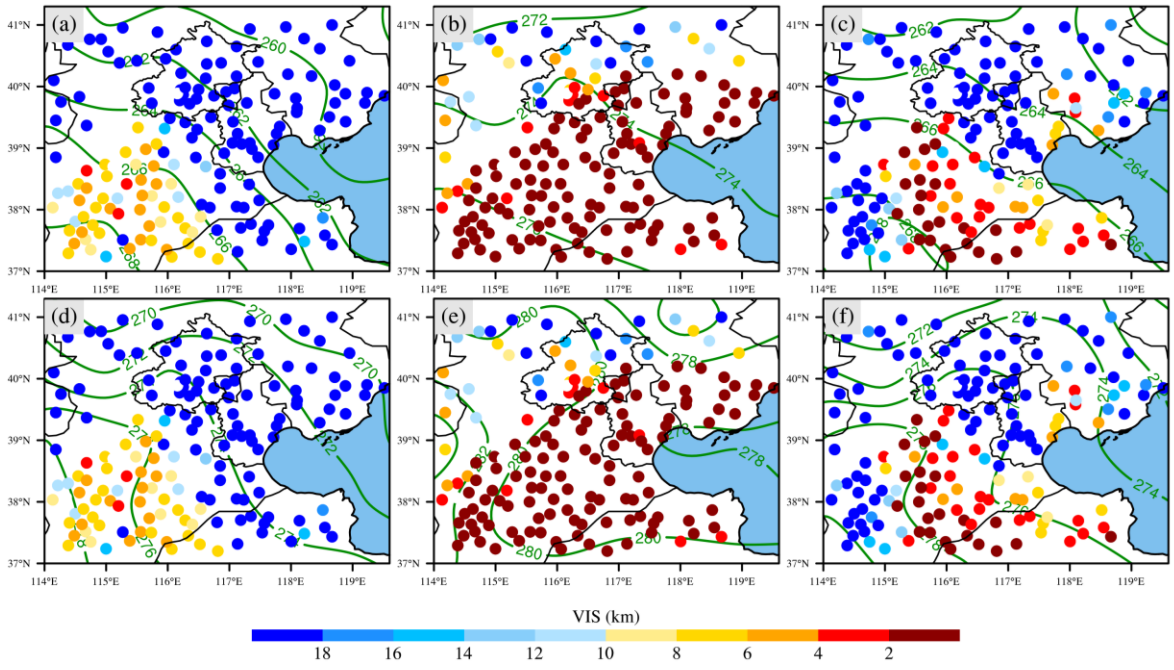

Figure 14. Similar to Figure 13, but for air temperature (K).

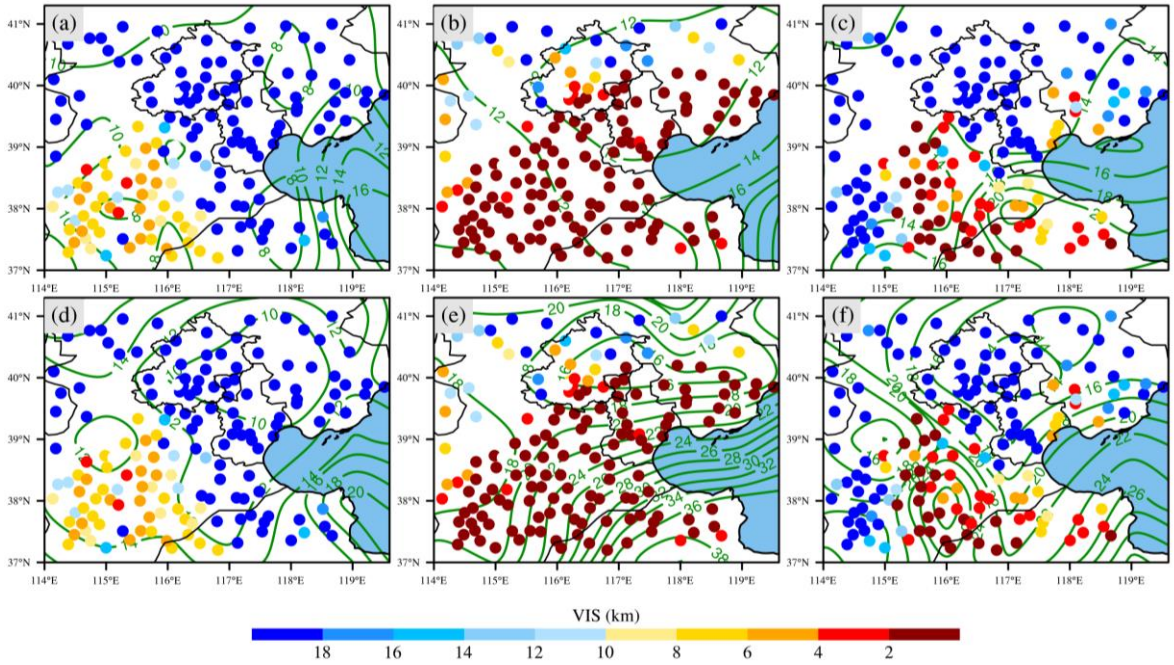

Figure 15. Similar to Figure 13, but for specific humidity (0.1 g kg^{-1}).

5.2. Meteorological Conditions Evolution

The above analysis reveals certain meteorological situation that corresponds to different evaluation stage for air pollution events. However, the evolution for meteorological conditions and foggy haze process is not clear yet. To explore this, the past 6-hour change of meteorological factors as well as the change of atmospheric visibility on the development (December 15), maintenance (December 18-21 with more than 80% ground station got visibility less than 2km) and dissipation (December 22) of foggy haze episode are discussed below.

The past 6-hour change of horizontal wind vertical shear (CWSH) as well as the change of atmospheric visibility (CAV) are showed in Figure 16. The development (at 2000 on December 15) and dissipation (at

1400 on December 22) stage of air pollution process is displayed in Figure 16 a-i, respectively. The variable change during air pollution maintenance period (from 1400 December 18 to 0200 December 21 with time interval of 12 hours) is shown in Figure 16 b-h. CWSH almost equal to zero during air pollution maintenance times despite the significant duration of visibility change (around 1 km at noon and -1 km at midnight), which indicates the diurnal variation of air pollutant concentration. Both at the beginning and end of an air pollution episode, CWSH showed an opposite trend to CAV, as the CWSH increased with CAV decrease at 2000 on December 15 and reduced with increased CAV at 1400 on December 22. This phenomenon is discrepant to the find on above section that wind shear decreased during pollution period. This contradiction may be introduced by the rapidly reduced/increased 850 hPa wind speed. In the beginning (pollution dissipation period), the 850 hPa wind speed decreased (increased) more rapidly than the wind speed at 500 hPa, and it caused the CWSH increase in the beginning and decrease in the end.

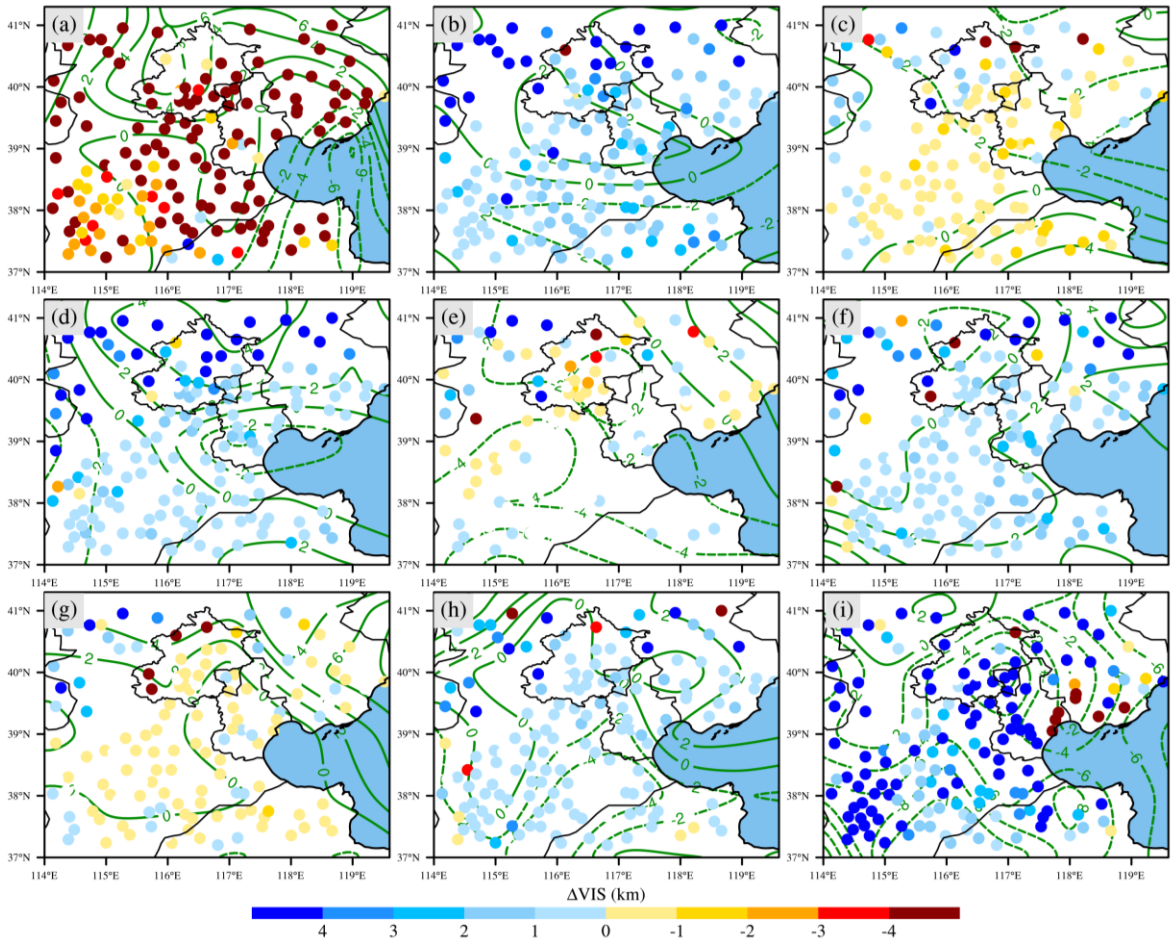

Figure 16. The past 6-hour change of horizontal wind vertical shear (ms^{-1}) and atmospheric visibility (km) in North China at 2000 on December 15 (a), December 18 1400 to December 21 0200 with time interval of 12 hours (b-i) and at 1400 on December 22 (j).

In contrast to the CWSH, the past 6-hour change of pseudo-equivalent potential temperature gradient (between 850 hPa and 1000 hPa, CPT) increased at air pollution in the beginning (Figure 17 a) while decreased during the pollution dissipation period (figure 17 i). This is consistent with the conclusions drawn in section 5.1. During foggy haze maintenance period shown in Figure 17 b-h, the CPT mostly reflected a inverse proportion to the CAV. In other words, the increased CPT always corresponded to decreased CAV, while decreased CPT corresponded to increased CAV. The only exception was for 0200 on December 20, which could be caused by the insignificant air temperature duration on this day (showed in Figure 2 c). The insignificant air temperature daily duration cut down the daily duration of visibility and the thermodynamic conditions. Nevertheless, on the other polluted day, the inverse correlation between CPT and CAV indicated the coupling thermodynamic conditions during foggy haze maintenance period. This can explain the significant correlation between daily evolutions of vertical difference of the pseudo-equivalent potential temperature gradient and atmospheric visibility shown in Figure 9.

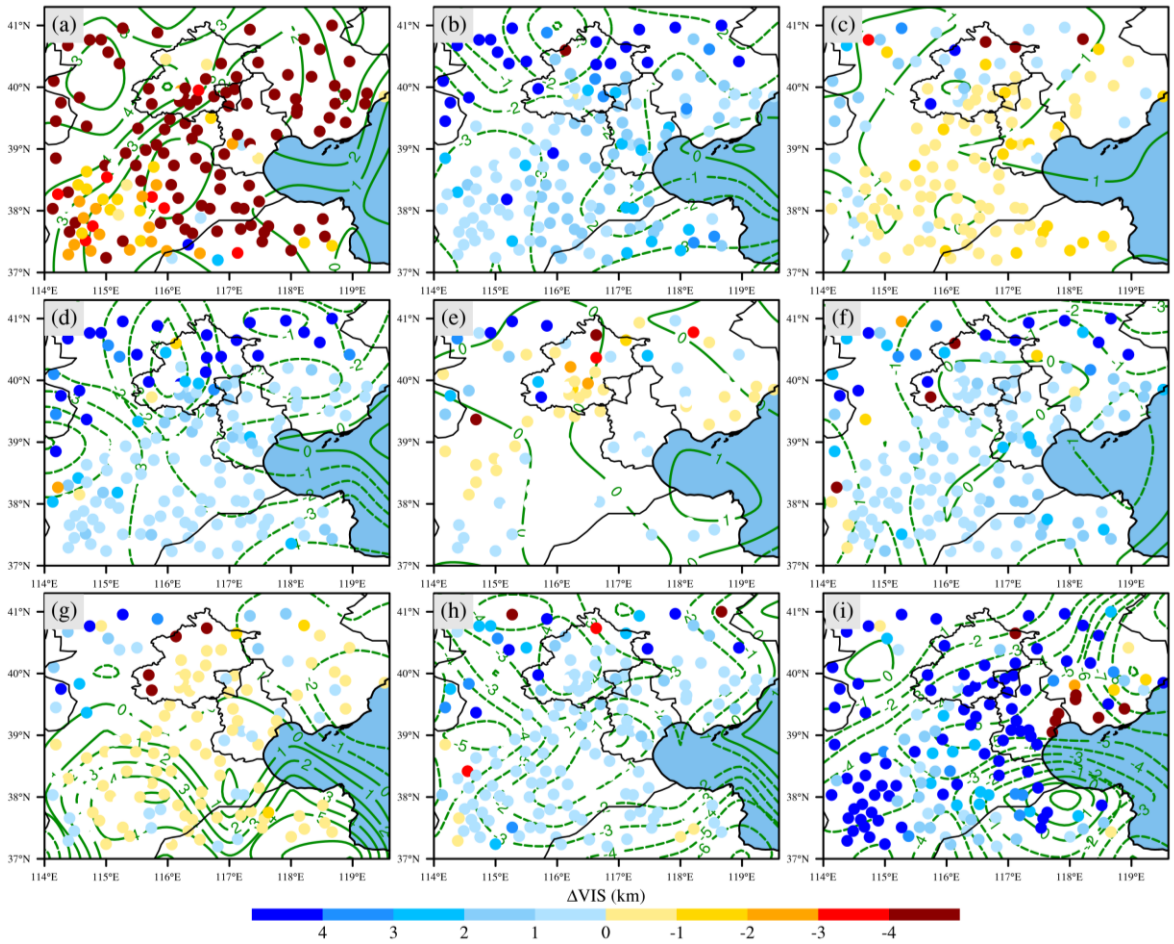

Figure 17. The past 6-hour change of pseudo-equivalent potential temperature gradient (K) and atmospheric visibility (km) in North China at 2000 on December 15 (a), December 18 1400 to December 21 0200 with time interval of 12 hours (b-i) and at 1400 on December 22 (j).

To further explore the key factor that affect the CPT during the pollution period, we analyzed the air temperature at 850 hPa and 1000 hPa as the slightly influence of specific humidity that found above. Figure 18-19 display the past 6-hour change of 1000 hPa (CT1000) and 850 hPa air temperatures (CT850) as well as the change of atmospheric visibility. At the foggy haze development stage, the increased CT850 with the decreased CAV demonstrate the warm effect of air pollutant once again with the slightly warm advection determined previously. At the same time, the decreased CT1000 indicates the radiation reduction effect of air pollutant. Similar to CPT, the CT1000 also showed an opposite correlation to CAV while CT850 did not. This significant (slightly) correlation between CT1000 (CT850) and CAV indicates that the significant correlation between CPT and CAV may be caused by CT1000, which means that the near surface air temperature controlled the thermodynamic conditions on the evolution of foggy haze episodes. The air pollutant affects the air temperature not only at near surface but also at middle and lower level [31-33], so this coupling air temperature and air pollutant structures creates appropriate thermodynamic conditions to foggy haze events with the atmospheric visibility less than 2 km.

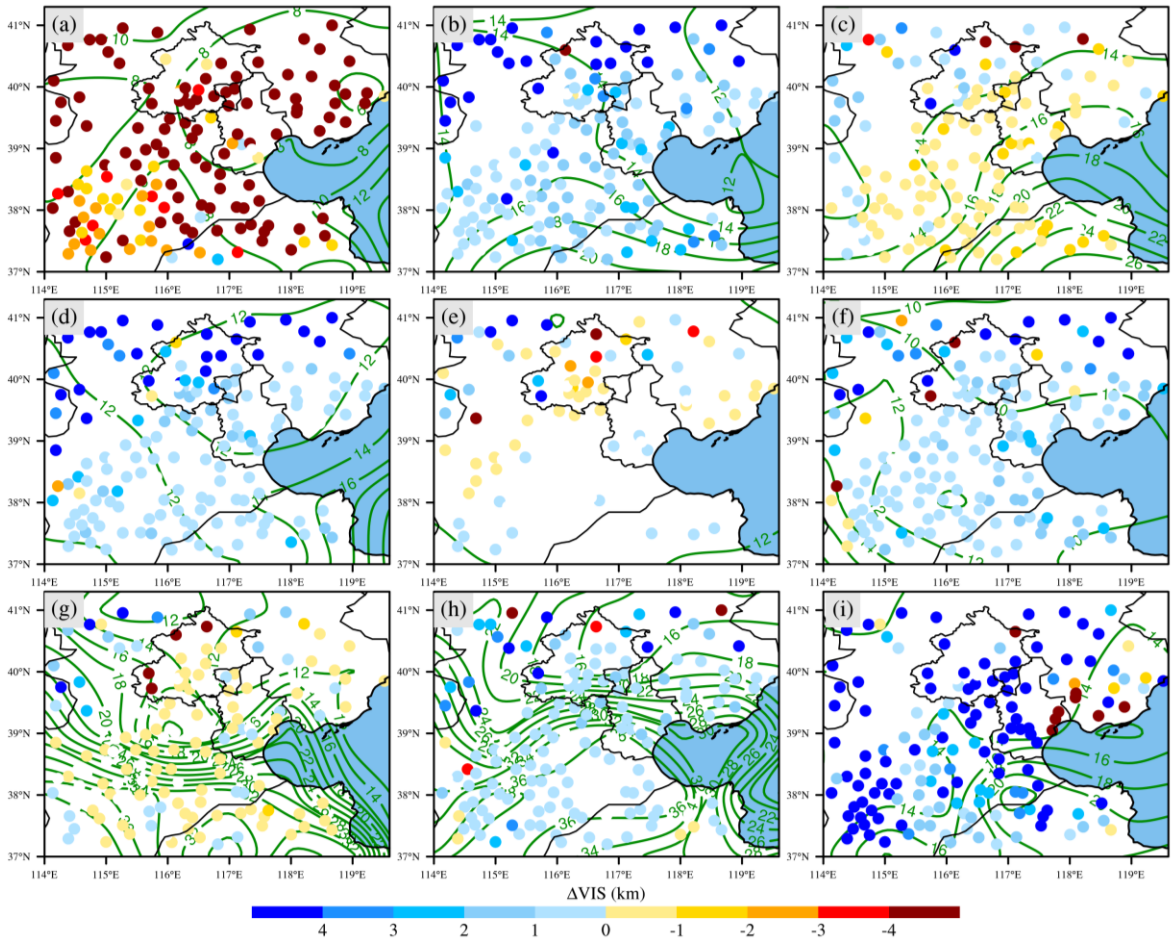

Figure 18. Similar to Figure 17 but for air temperature (K) at 850 hPa.

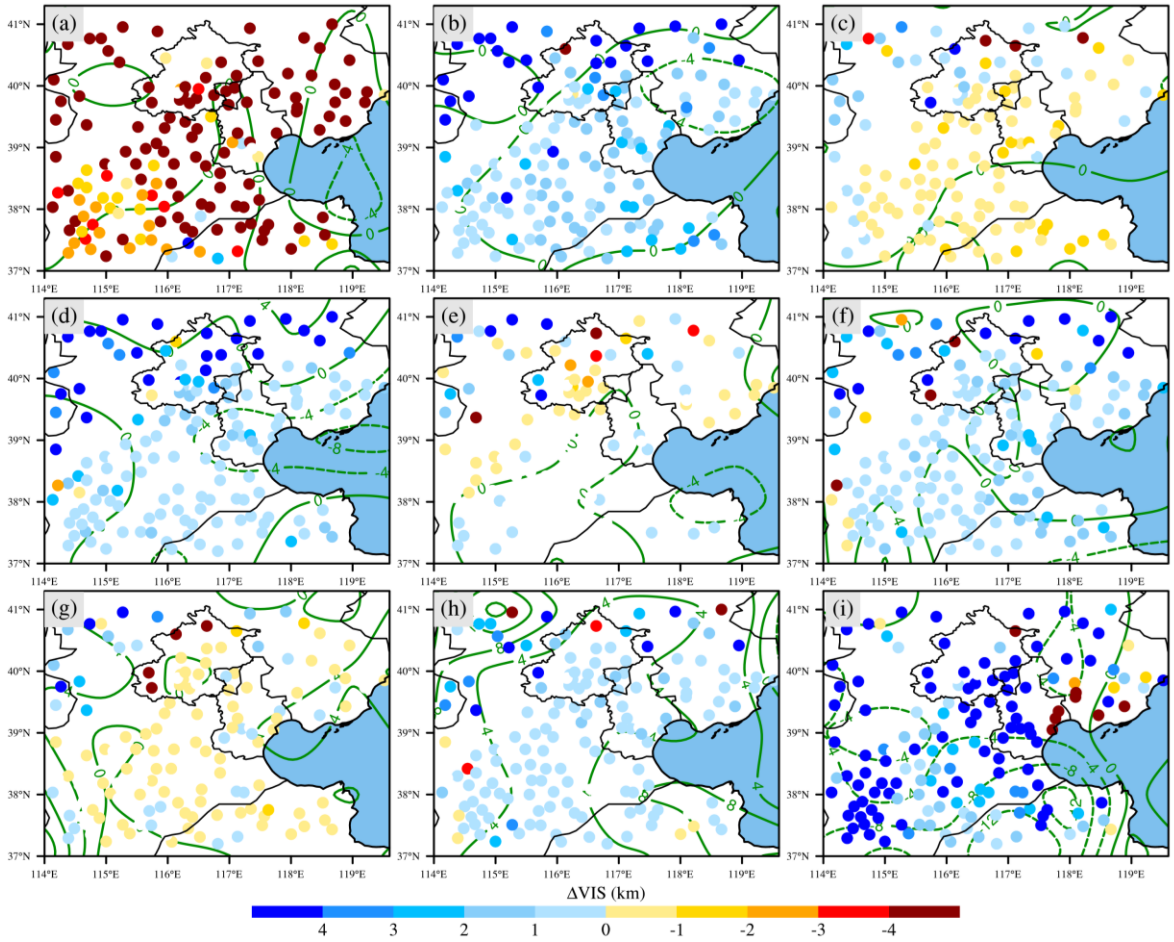

Figure 19. Similar to Figure 17 but for air temperature (K) at 1000 hPa.

The above analysis reflects the dynamic and thermodynamic conditions evolution as well as foggy haze episode from December 15 to 22, 2016. The 500 hPa decreased wind speed led to smaller horizontal wind vertical shear that weaken air exchange between difference levels. Meanwhile, air pollutants absorbed solar radiation [31-33], which increased air temperature at 850 hPa, and they reduced the radiation near surface. Despite the small warm advection at near surface, this decrease radiation effect formed a lower temperature at near surface. These stable thermodynamic conditions will again weaken the vertical movement and contribute to the accumulation of air pollutant near surface, causing high level air pollution events. The coupled air pollutant and thermodynamic situation provided favorable conditions for high level foggy haze events once there are air pollutant transport and weak vertical exchange conditions. Therefore, in this area, dynamic conditions are important, especially for weakened middle level wind speed and lower level south flow. As these dynamic conditions indicate an air pollution episode may happen in the next few days. Zhang et al [24] analyzed the dynamic and thermodynamic conditions in eastern China, and they found the significant influence of dynamic but less influence of thermodynamic. This may be attributed to the variable dynamic conditions in that area, which prevents the occurrence of coupled structure of air pollutant and thermodynamic configuration.

6. Summary

The impacts of the meteorological conditions on the foggy haze episodes were quantified by using 162 ground observation stations data and NCEP final analysis data in North China from December 1, 2016 to January 9, 2017. During this severe air pollution period, more than 72% of the regional mean atmospheric visibility was lower than 10 km. The minimum of the regional mean atmospheric visibility was only 1.15 km.

The atmospheric background field analysis implied that in lower troposphere southerlies and low wind speed were more conducive to the transportation of the southern pollutants to North China. Moreover, a high pressure in middle troposphere combined with the reduced temperature gradient in lower troposphere, suppress the local convection and lead to pollutants accumulation in the ground. This combination of weather

conditions in middle and lower troposphere may lead to heavy air pollution events. During the air pollution dissipation period, northerlies with a high wind speed quickly blows away the pollutant. However, relative humidity analysis shows that there is little influence of water vapor conditions on these foggy haze episodes.

The meteorological factors analysis suggests that the thermodynamic condition in lower troposphere significantly affects the evolution of foggy haze episodes in North China, while the middle and lower troposphere dynamic condition plays a second role. Stronger thermodynamic effect may be attributed to the stable dynamic conditions in North China than the eastern China. The insignificant influence of water vapor condition during this foggy haze episod is confirmed by the thermodynamic effect analysis. The multiple regression analysis suggests that the contribution of meteorological factors to the variance of daily foggy haze evolution reaches 79%, while more than 76 % can be explained by the thermodynamic effect.

The analysis on a foggy haze case during December 15-23 concludes that smaller horizontal wind vertical shear was caused by decreased wind speed at 500 hPa. Meanwhile, the air pollutant increased air temperature at 850 hPa and reduced air temperature near surface. This stable thermodynamic condition would again weaken the vertical movement and accumulate air pollutant near surface, which in turn, leads to a high level air pollution event. The coupled air pollutant concentration and thermodynamic situation evolution provided favorable conditions for heavy foggy haze episodes, especially when there were air pollutant transport and weak vertical exchange conditions. Therefore, it is suggested that, in this area, the favorable dynamic situation, such as weakened middle level wind speed and lower level south flow, indicate an air pollution episode may occur in the next few days.

Funding: This research was supported by grants from National Key Research and Development Program of Ministry of Science and Technology of China (2016YFC0203304), and National Natural Science Foundation of China (41875013, 41275022, and 41711530223).

Author Contributions: Zhiqiu Gao proposed the idea. Xin Li and Yubin Li processed the data and wrote the first draft. Chloe Y. Gao, Jingzheng Ren, and Xiaoye Zhang participated in the discussion and writing.

Conflicts of Interest: None.

References

[1] N. Bei, B. Xiao, N. Meng, and T. Feng, "Critical role of meteorological conditions in a persistent haze episode in the Guanzhong basin, China," *Sci Total Environ,* vol. 550, pp. 273-84, Apr 15 2016.

[2] C. K. Chan and X. Yao, "Air pollution in mega cities in China," *Atmospheric Environment,* vol. 42, pp. 1-42, 2008.

[3] H. Chen and H. Wang, "Haze Days in North China and the associated atmospheric circulations based on daily visibility data from 1960 to 2012," *Journal of Geophysical Research: Atmospheres,* vol. 120, pp. 5895-5909, 2015.

[4] Y. Ding, P. Wu, Y. Liu, and Y. Song, "Environmental and Dynamic Conditions for the Occurrence of Persistent Haze Events in North China," *Engineering,* vol. 3, pp. 266-271, 2017.

[5] Z. H. Chen, S. Y. Cheng, J. B. Li, X. R. Guo, W. H. Wang, and D. S. Chen, "Relationship between atmospheric pollution processes and synoptic pressure patterns in northern China," *Atmospheric Environment,* vol. 42, pp. 6078-6087, 2008.

[6] H. Zhao, H. Che, Y. Ma, Y. Wang, H. Yang, Y. Liu, *et al.*, "The Relationship of PM Variation to Visibility and Mixing Layer Height under Haze Fog Condition in Multi Cities of Northeast China," vol. 14, p. 471, 2017.

[7] X. J. Zhao, P. S. Zhao, J. Xu, W. Meng, W. W. Pu, F. Dong, *et al.*, "Analysis of a winter regional haze event and its formation mechanism in the North China Plain," *Atmospheric Chemistry and Physics*, vol. 13, pp. 5685-5696, 2013.
[8] G. Q. Fu, W. Y. Xu, R. F. Yang, J. B. Li, and C. S. Zhao, "The distribution and trends of fog and haze in the North China Plain over the past 30 years," *Atmospheric Chemistry and Physics*, vol. 14, pp. 11949-11958, 2014.
[9] L. Zhu, X. Huang, H. Shi, X. Cai, and Y. Song, "Transport pathways and potential sources of PM10 in Beijing," *Atmospheric Environment*, vol. 45, pp. 594-604, 2011.
[10] Y. Sun, T. Song, G. Tang, and Y. Wang, "The vertical distribution of PM2.5 and boundary-layer structure during summer haze in Beijing," *Atmospheric Environment*, vol. 74, pp. 413-421, 2013.
[11] W. Yang, G. Wang, and C. Bi, "Analysis of Long-Range Transport Effects on PM2.5 during a Short Severe Haze in Beijing, China," *Aerosol and Air Quality Research*, vol. 17, pp. 1610-1622, 2017.
[12] Y. Miao, J. Guo, S. Liu, H. Liu, G. Zhang, Y. Yan, *et al.*, "Relay transport of aerosols to Beijing-Tianjin-Hebei region by multi-scale atmospheric circulations," *Atmospheric Environment*, vol. 165, pp. 35-45, 2017.
[13] D. Ji, Y. Wang, L. Wang, L. Chen, B. Hu, G. Tang, *et al.*, "Analysis of heavy pollution episodes in selected cities of northern China," *Atmospheric Environment*, vol. 50, pp. 338-348, 2012.
[14] S. Han, H. Bian, X. Tie, Y. Xie, M. Sun, and A. Liu, "Impact of nocturnal planetary boundary layer on urban air pollutants: measurements from a 250-m tower over Tianjin, China," *J Hazard Mater*, vol. 162, pp. 264-9, Feb 15 2009.
[15] J. Quan, Y. Gao, Q. Zhang, X. Tie, J. Cao, S. Han, *et al.*, "Evolution of planetary boundary layer under different weather conditions, and its impact on aerosol concentrations," *Particuology*, vol. 11, pp. 34-40, 2013.
[16] X. G. Liu, J. Li, Y. Qu, T. Han, L. Hou, J. Gu, *et al.*, "Formation and evolution mechanism of regional haze: a case study in the megacity Beijing, China," *Atmospheric Chemistry and Physics*, vol. 13, pp. 4501-4514, 2013.
[17] Y. Miao, J. Guo, S. Liu, H. Liu, Z. Li, W. Zhang, *et al.*, "Classification of summertime synoptic patterns in Beijing and their associations with boundary layer structure affecting aerosol pollution," *Atmospheric Chemistry and Physics*, vol. 17, pp. 3097-3110, 2017.
[18] J. Chen, C. S. Zhao, N. Ma, P. F. Liu, T. Göbel, E. Hallbauer, *et al.*, "A parameterization of low visibilities for hazy days in the North China Plain," *Atmospheric Chemistry and Physics*, vol. 12, pp. 4935-4950, 2012.
[19] J. Quan, Q. Zhang, H. He, J. Liu, M. Huang, and H. Jin, "Analysis of the formation of fog and haze in North China Plain (NCP)," *Atmospheric Chemistry and Physics*, vol. 11, pp. 8205-8214, 2011.
[20] X. Ye, Y. Song, X. Cai, and H. Zhang, "Study on the synoptic flow patterns and boundary layer process of the severe haze events over the North China Plain in January 2013," *Atmospheric Environment*, vol. 124, pp. 129-145, 2016.

[21] J. Li, H. Chen, Z. Li, P. Wang, M. Cribb, and X. Fan, "Low-level temperature inversions and their effect on aerosol condensation nuclei concentrations under different large-scale synoptic circulations," *Advances in Atmospheric Sciences,* vol. 32, pp. 898-908, 2015.

[22] X. M. Hu, Z. Ma, W. Lin, H. Zhang, J. Hu, Y. Wang, *et al.*, "Impact of the Loess Plateau on the atmospheric boundary layer structure and air quality in the North China Plain: a case study," *Sci Total Environ,* vol. 499, pp. 228-37, Nov 15 2014.

[23] L. Wei, Z. Pu, and S. Wang, "Numerical Simulation of the Life Cycle of a Persistent Wintertime Inversion over Salt Lake City," *Boundary-Layer Meteorology,* vol. 148, pp. 399-418, 2013.

[24] R. Zhang, L. Qiang, and Z. RuoNan, "Meteorological conditions for the persistent severe fog and haze event over eastern China in January 2013," *Science China Earth Sciences,* vol. 57, pp. 26-35, 2013.

[25] X. Guo, T. Yang, S. Miao, and Y. Sun, "Urban Boundary-Layer Stability and Turbulent Exchange during Consecutive Episodes of Particle Air Pollution in Beijing, China," vol. 7, pp. 62-66, 2015.

[26] X. Zhuang, Y. Wang, H. He, J. Liu, X. Wang, T. Zhu, *et al.*, "Haze insights and mitigation in China: An overview," *Journal of Environmental Sciences,* vol. 26, pp. 2-12, 2014.

[27] K. Wang, H. Tian, S. Hua, C. Zhu, J. Gao, Y. Xue, *et al.*, "A comprehensive emission inventory of multiple air pollutants from iron and steel industry in China: Temporal trends and spatial variation characteristics," *Science of The Total Environment,* vol. 559, pp. 7-14, 2016.

[28] H. Wang, J. Xu, M. Zhang, Y. Yang, X. Shen, Y. Wang, *et al.*, "A study of the meteorological causes of a prolonged and severe haze episode in January 2013 over central-eastern China," *Atmospheric Environment,* vol. 98, pp. 146-157, 2014.

[29] D. Wu, X. Bi, X. Deng, F. Li, H. Tan, G. Liao, *et al.*, "Effect of atmospheric haze on the deterioration of visibility over the Pearl River Delta," *Acta Meteorologica Sinica,* vol. 21, p. 215, 2007.

[30] A. K. Showalter, "A stability index for thunderstorm forecasting," *Bull.amer.meteor.soc,* vol. 34, pp. 250-252, 1953.

[31] J. C. Dupont, M. Haeffelin, J. Badosa, T. Elias, O. Favez, J. E. Petit, *et al.*, "Role of the boundary layer dynamics effects on an extreme air pollution event in Paris," *Atmospheric Environment,* vol. 141, pp. 571-579, 2016.

[32] J. Xu, C. Li, H. Shi, Q. He, and L. Pan, "Analysis on the impact of aerosol optical depth on surface solar radiation in the Shanghai megacity, China," *Atmospheric Chemistry and Physics,* vol. 11, pp. 3281-3289, 2011.

[33] S. Wang, T. Liao, L. Wang, and Y. Sun, "Process analysis of characteristics of the boundary layer during a heavy haze pollution episode in an inland megacity, China," *J Environ Sci (China),* vol. 40, pp. 138-44, Feb 2016.

[34] C. Leng, J. Duan, C. Xu, H. Zhang, Y. Wang, Y. Wang, *et al.*, "Insights into a historic severe haze event in Shanghai: synoptic situation, boundary layer and pollutants," *Atmospheric Chemistry and Physics,* vol. 16, pp. 9221-9234, 2016.

608 [35] Y. Ding and Y. Liu, "Analysis of long-term variations of fog and haze in China in
609 recent 50 years and their relations with atmospheric humidity," *Science China Earth*
610 *Sciences*, vol. 57, pp. 36-46, 2013.

611